JPE 18-4-21

https://doi.org/10.6113/JPE.2018.18.4.1190
ISSN(Print): 1598-2092 / ISSN(Online): 2093-4718

Bi-Directional Wireless Power Transfer for Vehicle-to-Grid Systems

Yue Sun†, Cheng Jiang*, Zhihui Wang*, Lijuan Xiang*, and Huan Zhang*

†,*College of Automation, Chongqing University, Chongqing, China

Abstract

A current sourced bi-directional wireless power transfer (WPT) system is proposed to solve the problems that exist in the bi-directional WPT for vehicle-to-grid (V2G) systems. These problems include the fact that these systems are not safe enough, the output power is limited and the control methods are complicated. Firstly, the proposed system adopts two different compensation and control methods on both the primary and secondary sides. Secondly, based on an AC impedance analysis, the working principle is analyzed and the parameter configuration method with frequency stability is given. In order to output a constant voltage, a bi-directional DC/DC circuit and a controllable rectifier bridge are adopted, which are based on the "constant primary current, constant secondary voltage" control strategy. Finally, the effectiveness and feasibility of the proposed methods are verified by experimental results.

Key words: Bi-directional wireless power transfer, Compensation and control, Controllable rectifier bridge, Current source

I. INTRODUCTION

In wireless power transfer (WPT) systems, the bi-directional transmission of power is very important. It is useful for electric vehicles to achieve vehicle-to-grid (V2G) power so thier motors can realize four quadrant operation for feeding energy back to the supply and for improving the efficiency of systems [1]-[6].

At present, there are several common ways to set up a bi-directional WPT system. The authors of [7], [8] built a SS (Series-Series) type bi-directional WPT system. Its working frequency remains stable when the load resistance is changed, and it is easy to understand and achieve. The authors of [9]-[11] designed a bi-directional WPT system with LCL compensation on both sides. It has a larger resonant capacity, less device pressure, and frequency stability. The impedance transformation characteristics of LCL topology makes the resonant capacitor obtain high voltage. Moreover, the LCL topology increases the total reactive power. The two methods above are also used to achieve bi-directional WPT systems with a multi-load since they can keep the resonant frequency stable when the resistance of the load is changed [12], [13]. The authors of [14], [15] used a coil as an intermediary to increase the transmission distance. The PP (Parallel-Parallel) type can also be used in bi-directional WPT systems [16]. The authors of [17]-[18] used the RF (Radio Frequency) method to achieve bi-directional WPT systems.

The above methods can solve some problems. However, they also have some shortcomings. The main shortcomings of the SS and LCL-LCL type bi-directional WPT systems are as follows. First of all, as voltage sourced WPT systems, they are not as safe as current sourced ones. If the switching devices on the same inverter bridge arm are turned on at the same time the circuit is burned due to a control error or smearing effect. Second, most of the available control methods can only reduce the output voltage to remain stable, which makes the output power of these systems limited [8]-[11]. Third, some control methods request a signal exchange between the primary and secondary sides [15], [19]. This is complex and somewhat unreliable. Fourth, SS and LCL-LCL type compensation networks have no loop to release energy when the inverter bridge is stopped. Therefore, there is energy remaining in the coils and capacitors, which can be very dangerous. In addition, some methods are very complex to achieve [20]. Their applications are special, and they cannot remain in a stable working frequency by configuring parameters [16].

Manuscript received Sep. 15, 2017; accepted Feb. 5, 2018
Recommended for publication by Associate Editor M. Vilathgamuwa.
†Corresponding Author: syue@cqu.edu.cn
Tel: +86-65112750, Fax: +86-65112750, Chongqing University
*College of Automation, Chongqing University, Chongqing, China

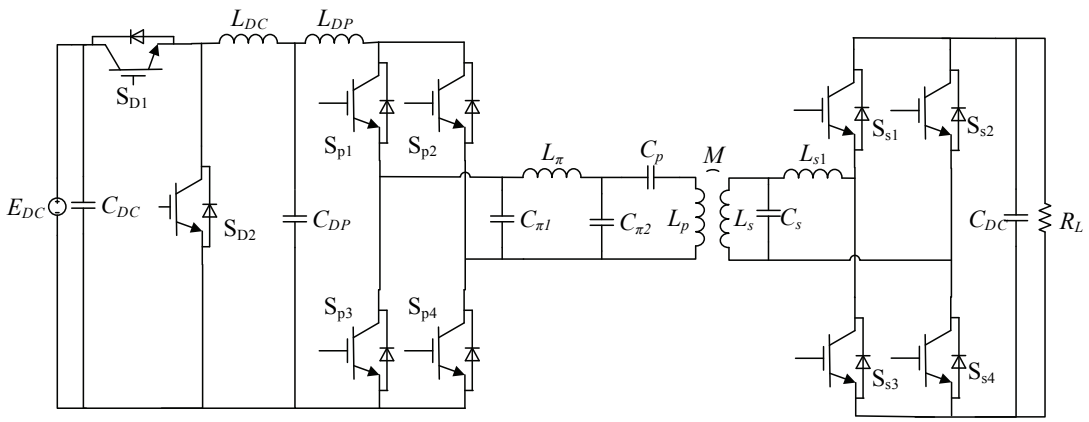

Fig. 1. Main circuit topology of the WPT system.

In this paper, a CLCS-LCL current sourced bi-directional WPT system is proposed, which has better security and power transfer capacity. It is the first system to take the different power characteristics of the primary and secondary sides into consideration. Moreover, a bi-directional DC/DC circuit and a controllable rectifier bridge are used. This makes it possible to realize the "constant primary current, constant secondary voltage" control strategy. This control strategy takes use of closed loop control independently on the primary and secondary sides. Therefore, it does not require information exchange, and is both stable and reliable.

This paper is organized as follows. The main circuit of the proposed current sourced bi-directional WPT system is presented in Section II. The control method is proposed in Section III. The advantages of the proposed methods are given in section IV. Experimental results are shown in Section V. Some conclusions are given in Section VI.

II. Topology Analysis and Establishing the Model of the System

A. Main Topology of the Proposed WPT System

The main topology of the bi-directional WPT system is shown in Fig. 1. This paper considers the left side as the grid and the right side as electric vehicles. Thus, the energy flows from the grid side to the electric vehicles side.

In Fig. 1, E_{DC} is the DC voltage source. A capacitor C_{DC}, switching devices S_{D1} and S_{D2}, an inductor L_{DC} and a capacitor C_{DP} make up the bi-directional DC/DC circuit. L_{DP} is a large-value inductor, and it is in series with the main circuit to make the input of the inverter bridge a quasi-current source. The inverter bridge is constituted by S_{P1}~S_{P4}. Then, L_π, $C_{\pi1}$ and $C_{\pi2}$ form the CLC compensated network, while C_P and L_P make up the series compensated network. An LCL network is adopted on the secondary side, which includes an energy pickup coil L_S, a capacitor Cs and an inductor L_{S1}. Four switching devices S_{S1}~S_{S4} form the high-frequency rectifier bridge. A large-value capacitor C_{DS} makes the output voltage stable, and R_L is the load resistor.

The load used on the secondary side is a pure resistor to simplify the analysis. When the system works in the V2G state, it is possible to exchange the load resistor and the input DC voltage source.

To conclude, this system takes a CLCS compensated network on the primary side, and an LCL compensated network on the secondary side. The reasons for this will be given below.

B. Parameter Configuration and Circuit Characteristics

In order to explore the parameter configuration methods and characteristics of the circuit, the AC impedance is used to analyze the system from the secondary side to the primary side.

According to the energy conservation law, when the devices in the circuit are ideal, the input power of the secondary rectifier is equal to its output power. Therefore, the AC equivalent resistance of the rectifier bridge and load resistor can be described as [21]:

$$R_{eq} = \frac{8}{\pi^2} R_L \tag{1}$$

Therefore, the compensation part can be equivalent to Fig. 2, as shown above. The whole impedance of the vehicle side can be shown as:

$$Z_S = j\omega L_S + (\frac{1}{j\omega C_S} // (j\omega L_{S1} + R_{eq})) \tag{2}$$

In this paper, "//" means parallel. Thus, the equivalent impedance after the CLC compensated network can be obtained as:

$$Z_{LC} = \frac{1}{j\omega C_P} + j\omega L_P + Z_r = \frac{1}{j\omega C_P} + j\omega L_P + \frac{\omega^2 M^2}{Z_S} \tag{3}$$

where, Z_r is the reflected impedance of the vehicle side, and M is the mutual inductance.

Therefore, the whole input impedance, seen from the inverter to the load, can be expressed as:

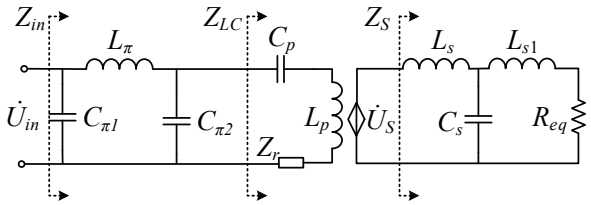

Fig. 2. Equivalent circuit of the compensation part for G2V.

$$Z_{in} = \frac{1}{j\omega C_{\pi1}} // (j\omega L_\pi + \frac{1}{j\omega C_{\pi2}} // Z_{LC}) \tag{4}$$

Z_S, Z_{LC} and Z_{in} are all shown in Fig. 2.

In order to make the system resonant, Z_S, Z_{LC} and Z_{in} should be purely resistive. According to (1)~(4), the parameters of the system should satisfy:

$$\omega = \frac{1}{\sqrt{L_\pi C_{\pi1}}} = \frac{1}{\sqrt{L_\pi C_{\pi2}}} = \frac{1}{\sqrt{L_P C_P}} = \frac{1}{\sqrt{L_S C_S}} = \frac{1}{\sqrt{L_{S1} C_S}} \tag{5}$$

Configuring the parameters based on (5) can make the soft switching frequency consistent with the resonant frequency. Thus, the system works in a good state. One more important thing to remember is that the working frequency is kept stable when the resistance of the load is changed. In addition, when the system transmits power from the vehicles to the gird, it has frequency stability. That is why two kinds of compensated networks are selected.

The primary CLC compensation network can amplify the input voltage, which can be calculated by:

$$\frac{\dot{U}_{C_{\pi2}}}{\dot{U}_{C_{\pi1}}} = \frac{\frac{1}{j\omega C_{\pi2}} // Z_{LC}}{j\omega L_\pi + (\frac{1}{j\omega C_{\pi2}} // Z_{LC})} = \frac{Z_{LC}}{j\omega L_\pi} \tag{6}$$

The induced voltage caused by the current flowing through the primary energy coil can be calculated by:

$$\dot{U}_S = j\omega M \dot{I}_P = \frac{j\omega M \dot{U}_{C_{\pi2}}}{Z_r} \tag{7}$$

Finally, the LCL compensation network on the vehicle side can also amplify the input voltage, which can be calculated by:

$$\begin{aligned} \frac{\dot{U}_{R_{eq}}}{\dot{U}_{R_{eq}}} &= \frac{\frac{1}{j\omega C_S} // (j\omega L_{S1} + R_{eq})}{j\omega L_S + \frac{1}{j\omega C_S} // (j\omega L_{S1} + R_{eq})} \times \frac{R_{eq}}{j\omega L_{S1} + R_{eq}} \\ &= \frac{R_{eq}}{j\omega L_S} \end{aligned} \tag{8}$$

For the V2G mode, the compensation part can be expressed by Fig. 3. The vehicle side adopts the LCL compensation network, and the current (i_{Ls}) is constant and independent of the load [22]:

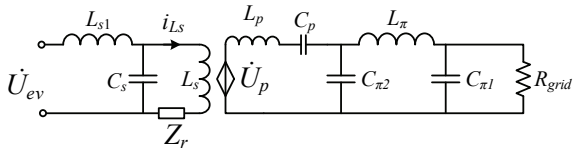

Fig. 3. Equivalent circuit of the compensation part for V2G.

TABLE I
PARAMETERS OF THE MAIN CIRCUIT

Parameters	Values
Input DC voltage E_{DC}(V)	24
Primary energy coil L_P(μH)	28.68
Primary equivalent series resistance R_P(Ω)	0.07
Primary compensation capacitor C_P(μF)	0.552
Primary CLC capacitors $C_{\pi1}$, $C_{\pi2}$(μF)	2
Primary CLC inductor L_π(μH)	7.92
Mutual inductance M(μH)	18.7
Secondary energy coil L_S(μH)	44.18
Secondary equivalent series resistance R_S(Ω)	0.09
Secondary compensation capacitor C_S(μF)	0.716
Secondary compensation inductor L_{S1}(μH)	44.18
Working frequency f(kHz)	40

$$i_{Ls} = \frac{\dot{U}_{ev}}{j\omega L_s} \tag{9}$$

The induced voltage can be shown as:

$$\dot{U}_p = j\omega M i_{Ls} = \frac{\dot{U}_{ev} M}{L_s} \tag{10}$$

Thus, the voltage of the grid side can be calculated as:

$$\frac{\dot{U}_{grid}}{\dot{U}_p} = \frac{\frac{1}{j\omega C_{\pi1}} // R_{grid}}{j\omega L_\pi + \frac{1}{j\omega C_{\pi1}} // R_{grid}} = \frac{R_{grid}}{j\omega L_\pi} \tag{11}$$

The parameter configuration methods and the characteristics between the input and output voltage have been completely discussed. All of the variables in the equations can be found in Fig. 1, Fig. 2 and Fig. 3.

According to the methods above, the parameters of the system are listed in Table 1.

C. The Working Principle of G2V and the Primary Control Method

To simplify the analysis, the rectification of industrial power is neglected, and the input of the system is directly considered as a DC voltage source.

The circuit before the primary inverter bridge is a bi-directional DC/DC circuit, as shown in Fig. 1. This circuit works in the buck state from the grid to electric vehicles, and in boost state it works in reverse. In the buck state, the

switching device S_{D1} is kept working. The switch S_{D2}, whose anti-parallel diode is working as a freewheeling diode, is kept off. The output voltage of the bi-directional DC/DC circuit is the voltage on the capacitor C_{DP} in Fig. 1. This is also the input voltage of the high-frequency inverter bridge. The relationship between this voltage and the input voltage E_{DC} can be expressed as:

$$U_{C_{DP}} = \frac{t_{on}}{t_{on} + t_{off}} E_{DC} = \alpha E_{DC} \tag{12}$$

where α is the on-duty of the switching device S_{D1}.

The input of the inverter bridge is in series with a big-value inductor. As a result, the value of the current does not change abruptly. Therefore, the input can be seen as a quasi-current source. When all of the parameters are configured by (5), the input impedance is purely resistive. Considering that the switching devices are ideal, the input and output power of the inverter bridge should be equal. Therefore, the output voltage of the inverter bridge can be calculated by [23]:

$$U_{C_{\pi 1}} = \frac{\pi}{2\sqrt{2}} U_{C_{DP}} \tag{13}$$

According to (6)-(8), the output voltage of the system u_{out} can be regulated by changing the duty ratio α of S_{D1}.

However, this method is not adopted in this paper since it relies on the exchange of information between the primary and secondary sides, and the output power is restricted by a buck circuit, which can only reduce the output power. In order to overcome the above shortcomings, a control strategy based on "constant primary current, constant secondary voltage" is utilized.

The output current of the CLCS network is constant and independent of the load [23,24]. Therefore, the current in the primary energy coil can be expressed as:

$$\dot{I}_{L_P} = \frac{U_{C_{\pi 1}}}{j\omega L_\pi} = \frac{\pi \alpha E_{DC}}{2\sqrt{2} j\omega L_\pi} \tag{14}$$

As it can be seen in (14), the current I_{Lp} can be controlled by regulating the duty ratio α of S_{D1} in the bi-directional DC/DC circuit.

III. Output Voltage Control Method

A. Independent Boost of the Controllable Rectifier Bridge

The parameter configuration methods, the working principle of the main circuits and the control method of primary circuit are discussed in the last section. As for the regulation of the output voltage on the secondary side, the existing methods are as follows. First, the DC/DC circuit can be added on the secondary side. Second, it is possible to design an additional signal channel to change the current in the primary energy coil. Finally, it also needs signal exchange between the primary and secondary sides, and depends on amplitude modulation or phase modulation on the primary side to keep the output voltage constant.

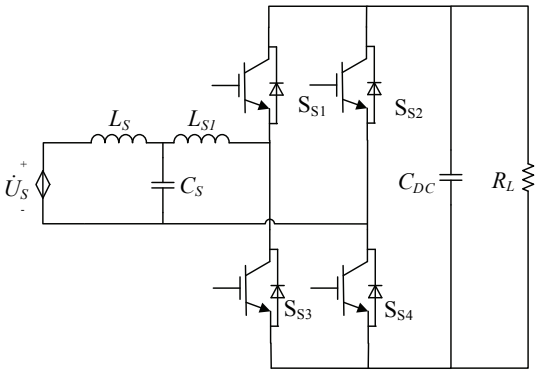

Fig. 4. Equivalent circuit of the vehicle side.

However, the vehicle side has less space and carrying capacity. If extra an DC/DC circuit is added, it increases the cost. If the signal from the secondary side is used for control, it increases the complexity and reduces the reliability. In addition, it is also very complicated. This paper takes the characteristics of the vehicle side into consideration and uses the independent boost of the controllable rectifier bridge as a control method to keep the output voltage constant.

According to the control method of the primary side, the current in the primary energy coil is constant. When the working angular frequency and mutual inductance of the system are kept stable, the induced voltage on the secondary side can be expressed as:

$$\dot{U}_S = j\omega M \dot{I}_{L_P} \tag{15}$$

Therefore, the equivalent circuit of the vehicle side can be drawn as Fig. 4.

From this point on, the vehicle side can be discussed independently. When compared with common WPT systems, the diodes are replaced with switching devices in Fig. 4. Meanwhile, an LCL compensation network is adopted. The output voltage can be regulated by controlling the switches S_{S3} and S_{S4}. Usually, the pickup voltage is lower than the expected voltage. Therefore, boost is considered in this paper. In addition, the output current can be controlled by the voltage regulation. The only difference is that the signal feeding back to the MCU is the current signal.

B. Analysis of the Working Principle

One current cycle is separated into 4 parts, and the working principle of every part is shown in Fig. 5. Each of the parts is discussed independently.

In Fig. 5, the upper left corner of each part shows the current flowing through the secondary coil L_{SI}, and the rest shows the circuit topology. The solid black line represents the wires and devices that are working, while the dotted black shows those that are not working. The dotted red line shows the direction of the current.

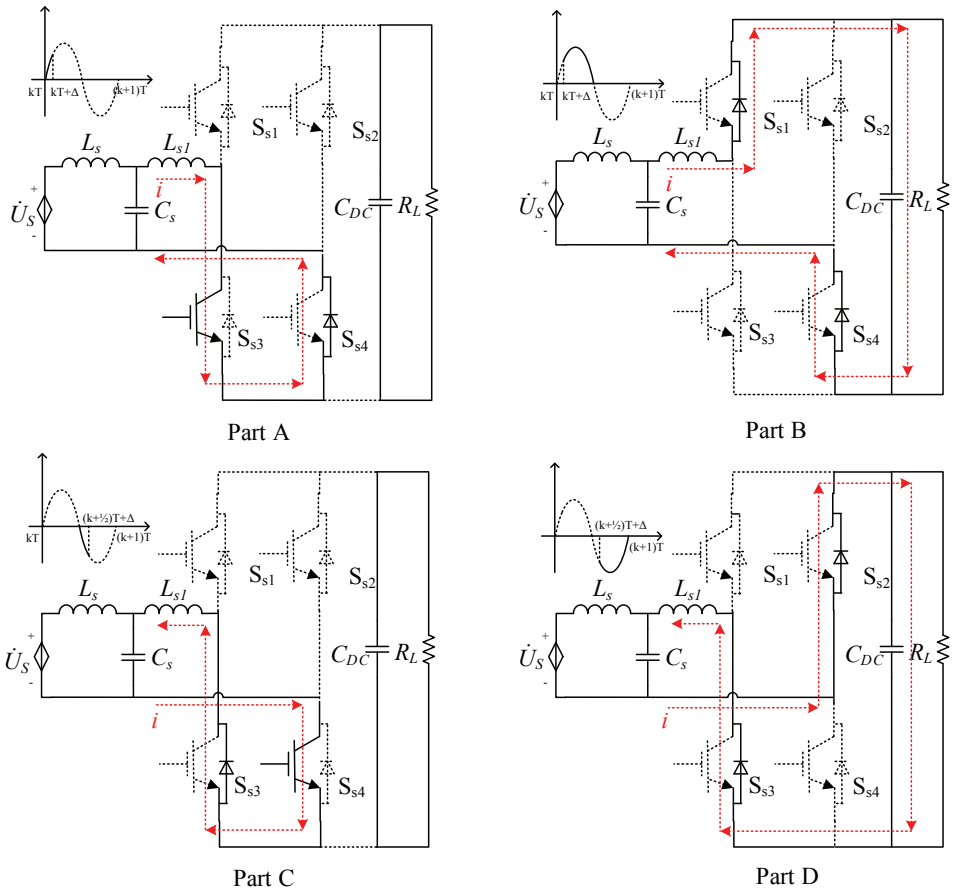

Fig. 5. Working principle of the circuits for different parts.

Part A [kT~(kT+Δ)]: this part begins from the zero crossing point of the positive half-wave, and ends at (kT+Δ). At this time, the switching device S_{S3} is turned on. The loop consists of the source U_S, the inductors L_S and L_{S1}, the capacitor C_S, the switch S_{S3} and the anti-parallel diode of S_{S4}. During this process, the inductors are charging by the source U_S to store energy, and the power for the load R_L is provided by the big-value capacitor C_{DC}.

Part B [(kT+Δ)~(k+1/2)T]: this part begins at the ending of part A, and ends at the ending of the positive half-wave. At this time, the switch S_{S3} is off. The loop consists of the source U_S, the inductors L_S and L_{S1}, the capacitor C_S, the anti-parallel diode of S_{S1}, the anti-parallel diode of S_{S4}, the big-value capacitor C_{DC} and the load R_L. During this process, the source U_S and the inductors provide energy to the load R_L and charge C_{DC}, together. That is why C_{DC} can provide power to the load in the next part.

Part C [(k+1/2)T~ (k+1/2)T+Δ]: this part begins at the ending of part B, and ends at (k+1/2)T+Δ. The switching device S_{S4} is on. The loop consists of the source U_S, the inductors L_S and L_{S1}, the capacitor C_S, and the switches S_{S3} and S_{S4}. During this process, the inductors are charging by the source U_S to store energy, and the power for the load R_L is provided by the big-value capacitor C_{DC}.

Part D [(k+1/2)T+Δ~(k+1)T]: this part begins at the ending of part C, ends at the ending of the negative half-wave. At this time, the switch S_{S4} is off. The loop consists of the source U_S, the inductors L_S and L_{S1}, the capacitor C_S, the anti-parallel diode of S_{S2}, the anti-parallel diode of S_{S3}, the big-value capacitor C_{DC} and the load R_L. During this process, the source U_S and the inductors provide energy to the load R_L and charge C_{DC}.

The working state of the system during a cycle is analyzed completely. In the following time, the working principle is the same as the analysis above. It is kind of similar to the traditional boost circuit, which is also charging the inductors to make them supply the load and the source together. Therefore, the output voltage of the system can be increased.

C. *Control Strategy Based on "Constant Primary Current, Constant Secondary Voltage"*

To conclude the control strategy in this paper, it can be expressed as "constant primary current, constant secondary voltage". This means keeping the current of primary energy coil and the output voltage of the secondary load constant at the same time.

The primary is the grid side. There are more space and less weight or volume limits. Therefore, bi-directional DC/DC

circuits are used to control the primary current. Although more hardware circuits are used, it is simple and practical. Meanwhile, the grid side requires more safety precautions. Therefore, a current sourced inverter is used. It is a lot safer than a voltage sourced inverter.

The secondary side is the vehicle side, which has a smaller space and more requirements in terms of weight and volume. Therefore, independent boost of the controllable rectifier bridge is used. This control method makes the output of the system constant and does not require any additional circuits.

Finally, to make sure the strategy of "constant primary current, constant secondary voltage" comes true, closed loop feedback is adopted. On the grid side, the current signal of the energy coil is fed back to the primary MCU. By regulating the duty ratio α of the bi-directional DC/DC circuit, the primary current is under control. On the vehicle side, the voltage of the load is fed back to the secondary MCU. This makes the voltage constant by controlling the duty ratio of the switching devices.

IV. Advantages of the Proposed System

This paper adopts a current sourced inverter, a CLCS-LCL compensation network, a bi-directional DC/DC circuit and independent boost of the controllable rectifier bridge to achieve a bi-directional WPT system for V2G. The advantages of these elements are explained below.

A. The Advantages of the Current Sourced Inverter

There are mainly two kinds of inverters in WPT systems. They are voltage sourced inverter and current sourced inverter. For the full bridge inverter in this paper, the only difference is that the input of the current sourced inverter is in series with a big-value inductor.

The big-value inductor suppresses abrupt change of the current. Therefore, the input current can be considered as relatively stable.

The big-value inductor also makes the system safer. For a practical circuit system, there is a time-delay problem of the driving signal and a smearing effect of the switching devices. Therefore, it is possible that the switching devices on the same inverter bridge arm are turned on at a certain moment. If a current sourced inverter is adopted, this problem is suppressed by the big-value inductor, and there is no danger. However, if this problem occurs in a voltage-fed inverter, the switching devices are directly burned.

The primary side is the grid. Therefore, safety should be taken into serious consideration. Therefore, the current sourced inverter is adopted in this paper.

B. The Advantages of the Compensation Network

There are different kinds of common compensation networks, such as SS [20], LCL-LCL [22] and LCC-LCC [25] networks. In this paper, a CLCS-LCL network is proposed. To make it clear, these compensation networks are drawn together, in Fig. 6.

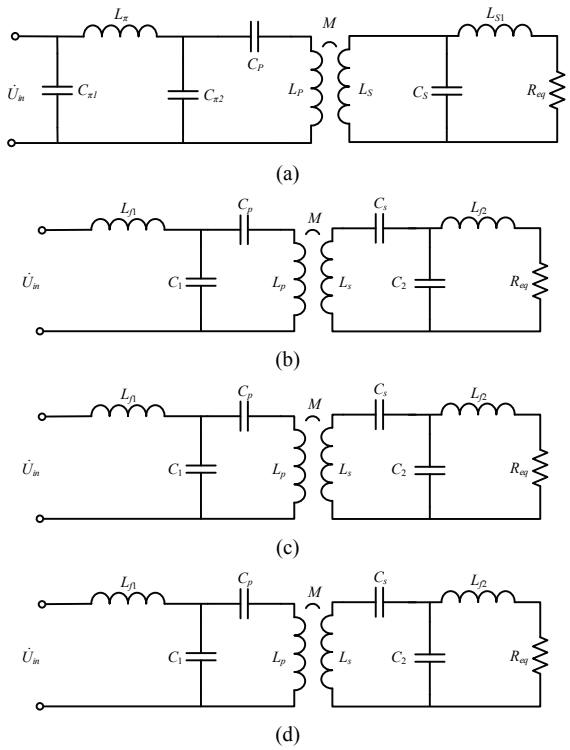

Fig. 6. Comparison of different topologies: (a) CLCS-LCL network proposed in this paper; (b) LCC-LCC network; (c) LCL-LCL network; (d) S-S network.

A number of different types of networks are shown in Fig. 6. The advantages of the proposed compensation network include the following benefits.

The first is the frequency stability. In a practical WPT system, the load resistor is always variable. According to (1)-(5), the resonant frequency of the CLCS-LCL network remains stable when the load resistance is changed.

The second is the discharge circuit. When the system stops working, the switching devices of the inverter bridge are turned off, and there is some energy remaining in the coupling coils and the compensation capacitors. As can be seen in Fig. 6(a), the CLCS-LCL network itself has the discharge circuit, and the remaining energy can be consumed by the internal resistor of the CLCS-LCL network. However, as can be seen in Fig. 6(b), 6(c) and 6(d), the LCC-LCC, LCL-LCL and S-S networks do not have a discharge circuit. Therefore, they can present a serious danger (LCC, LCL and S-S networks do not have a discharge channel. As a result, they can present a serious danger if the system does not take an extra control method or an extra discharge channel when the system stops running).

The third is the removal of the secondary side. The circuit from the secondary coil L_S to the load resistor is installed on electrical equipment, such as the electric vehicles in this

TABLE II
PERFORMANCE COMPARISON OF DIFFERENT COMPENSATION TOPOLOGIES

Type	S-S	LCL-LCL	LCC-LCC	CLCS-LCL
Input impedance	$\frac{\omega^2 M^2}{R_{eq}}$	$\frac{\omega^2 L_p^2 L_s^2}{M^2 R_{eq}}$	$\frac{\omega^2 L_{f1}^2 L_{f2}^2}{M^2 R_{eq}}$	$\frac{\omega^2 L_\pi^2 L_s^2}{M^2 R_{eq}}$
Voltage ratio	$\frac{jR_{eq}}{\omega M}$	$\frac{MR_{eq}}{j\omega L_p L_s}$	$\frac{MR_{eq}}{j\omega L_{f1} L_{f2}}$	$\frac{MR_{eq}}{j\omega L_s L_\pi}$
Output power	$\frac{U_{in}^2 R_{eq}}{\omega^2 M^2}$	$\frac{U_{in}^2 M^2 R_{eq}}{\omega^2 L_p^2 L_s^2}$	$\frac{U_{in}^2 M^2 R_{eq}}{\omega^2 L_{f1}^2 L_{f2}^2}$	$\frac{U_{in}^2 M^2 R_{eq}}{\omega^2 L_s^2 L_\pi^2}$

(a)

Type	Efficiency
S-S	$\frac{\omega^2 M^2 R_{eq}}{(R_{eq}+R_s)(R_{eq}R_p + R_p R_s + \omega^2 M^2)}$
LCL-LCL	$\frac{\omega^4 M^2 R_{eq} L_s^2}{\left(\omega^2 M^2 R_{eq} + R_p \omega^2 L_s^2 + R_p R_s R_{eq}\right)\left(R_s R_{eq} + \omega^2 L_s^2\right)}$
LCC-LCC	$\frac{\omega^4 M^2 R_{eq} L_{f2}^2}{\left(\omega^2 M^2 R_{eq} + R_p \omega^2 L_{f2}^2 + R_p R_s R_{eq}\right)\left(R_s R_{eq} + \omega^2 L_{f2}^2\right)}$
CLCS-LCL	$\frac{\omega^4 M^2 R_{eq} L_s^2}{\left(\omega^2 M^2 R_{eq} + R_p \omega^2 L_s^2 + R_p R_s R_{eq}\right)\left(R_s R_{eq} + \omega^2 L_s^2\right)}$

(b)

paper, and they are movable. Therefore, when the secondary circuit is removed, the input impedance only remains in the inner resistance of the primary compensation network. The primary circuit with series compensation can be directly burned. However, the primary current of a CLCS-LCL type WPT system can be kept stable, according to (14), and that keeps the system safe. Meanwhile, other networks such as the S-S cannot.

The fourth is the performance. A comprehensive comparison with regards to different compensation topologies is shown in Table II.

For the sake of simplification, this paper does not consider the coil resistance in Table II (a). However, it involves the efficiency analysis, while Table II (b) considers the internal resistance of the primary coil and secondary coil [23]-[25].

According to Table II, the voltage ratio, output power and efficiency of the different compensation topologies can be drawn as Fig. 7.

As can be seen, the proposed CLCS-LCL type WPT system can output a higher voltage and a higher power under the same conditions. In addition, the proposed topology can maintain a higher efficiency than the LCC-LCC and S-S topologies.

Fig. 7(a) shows the voltage ratio without any control methods. However, the proposed control method in this paper can raise the voltage. Meanwhile, other methods such as the "phase shift control" in [7] can only reduce the voltage.

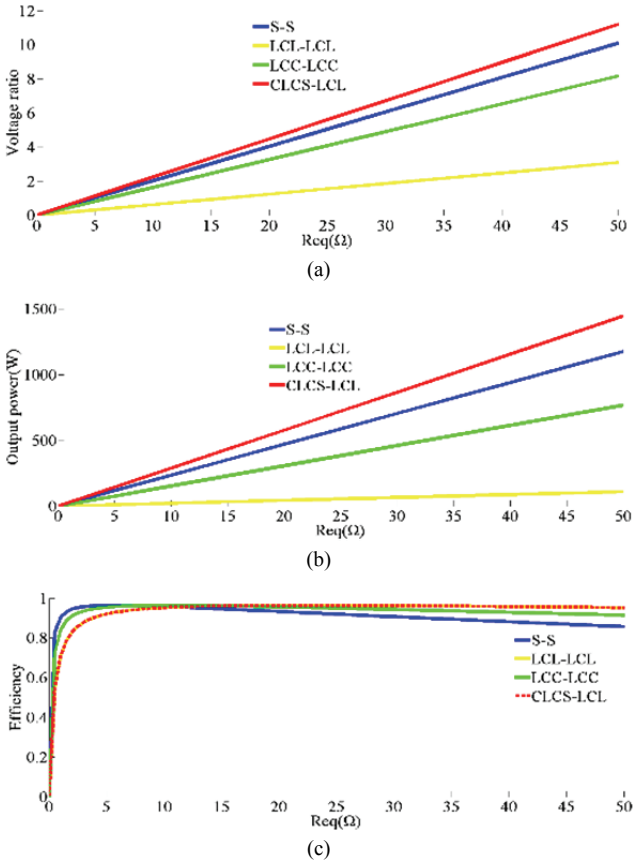

Fig. 7. Comparison of different compensation topologies: (a) Voltage ratio; (b) Output power; (c) Efficiency.

TABLE III
PARAMETER COMPARISON

Efficiency	Component Count	Driver Technology	Ref.
91%	4	Half Bridge	[7]
-	4	Full Bridge	[8]
85%	6	Full Bridge	[9]
-	6	Full Bridge	[10]
-	6	Full Bridge	[11]
88%	8	Full Bridge	[our work]

In addition, the system efficiency and component count are compared with previously publications, as shown in Table III.

The authors of [7] adopted a variable phase shift function to obtain the maximum efficiency. The system reaches a maximum efficiency of 91% at around 700W. However, when the output power is 200W, the efficiency is 82%.

From the above analysis, the CLCS-LCL topology has better performance than others.

C. *The Advantages of the Control Method*

In this paper, the primary side takes the bi-directional DC/DC circuit, and the secondary side takes the independent boost of the controllable rectifier bridge. The control strategy is "constant primary current, constant secondary voltage."

The advantages of the primary side are as follows. First, the bi-directional DC/DC circuit works in the buck state from the grid to vehicles, and boost state works form vehicles to the grid. The buck state can make the output reduce to zero. Thus, the no-load loss can be reduced.

Second, the boost state can increase the power from vehicles to the grid, while other control methods cannot.

Third, the bi-directional DC/DC circuit has more power conversion capability when compared with the control methods in [7]-[15].

The advantages of the secondary side mainly include two aspects. One is that this method does not add a main circuit. Thus, it results in savings in terms of cost and space. The other is that the independent boost of the controllable rectifier bridge can increase the output voltage. Meanwhile, almost all of the other control methods cannot [20].

There are independent closed loop feedbacks on both sides. Therefore, the system can be controlled without communication between the gird and vehicles, which saves a lot of cost and space. This control strategy makes the system simple, stable and reliable.

V. Experimental Study

In order to verify the effectiveness and feasibility of the system in this paper, an experiment platform has been built according to Fig. 1 and Table I, as shown in Fig. 8. The primary coil is 5cm×5cm, the secondary coil is 5.5cm×5.5cm and the resonant capacitance uses non-inductive capacitance.

Fig. 9 shows inverter and output voltage experimental waveforms of the system. As can be seen, the current i_{Lp} is quasi sine, and the phase difference between i_{Lp} and the driving waveform u_{GS} is 90°.

As can be seen in Fig. 10, the load is switched twice. First it is switched from 10Ω to 20Ω, and then back to 10Ω. However, the current in the primary coil i_{Lp} is kept stable. Therefore, the primary control is realized.

As can be seen in Fig. 11, when the secondary control starts, the output voltage increases and the primary current is kept stable. When the secondary control ends, the output voltage decreases, and the primary current is also kept the same.

According to (6)-(8), the output voltage can be calculated and its value is approximately 56V. In Fig. 11, the output voltage is approximately 52V when the secondary side does not have control action. There is a voltage deviation due to not considering the coil resistance in the theoretical analysis. Therefore, the experimental results have demonstrated the correctness of the theoretical analysis. Moreover, the output voltage increases to approximately 82V when the secondary side has control actions. Thus, the results have demonstrated the validity of the proposed methods of section III.

As can be seen in Fig. 12, when both the primary and

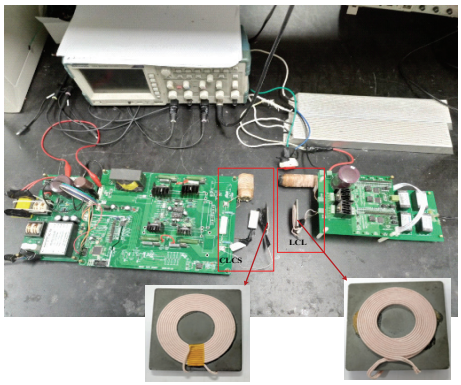

Fig. 8. Experimental setup of the system.

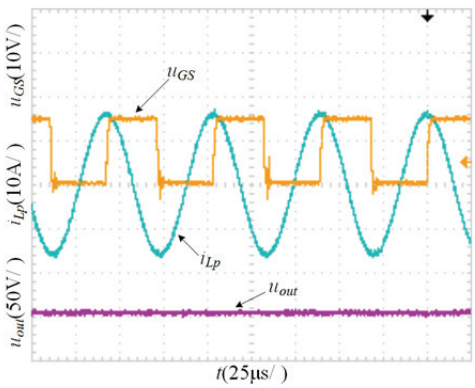

Fig. 9. Inverter and output voltage waveforms of the system.

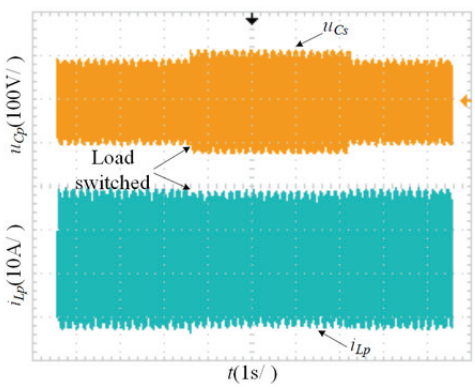

Fig. 10. Experimental waveforms of constant primary current.

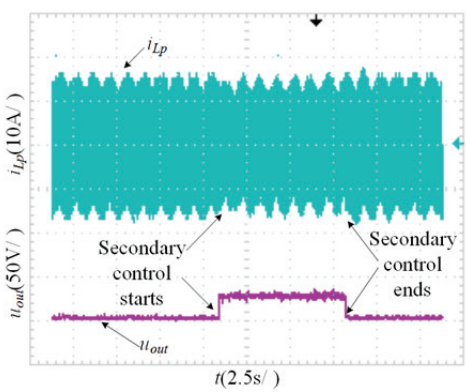

Fig. 11. Experimental waveforms of the secondary boost.

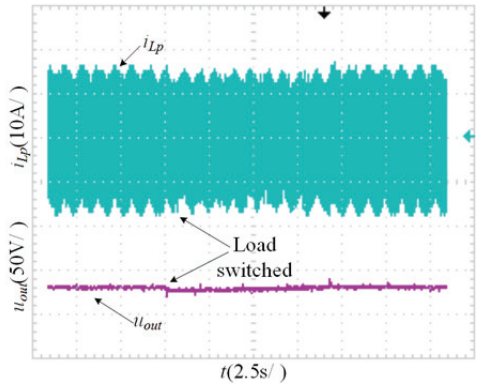

Fig. 12. Waveforms of the constant secondary voltage.

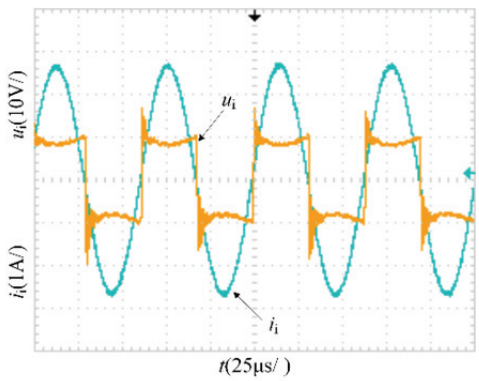

Fig. 13. Inverter waveforms from the vehicle to the grid.

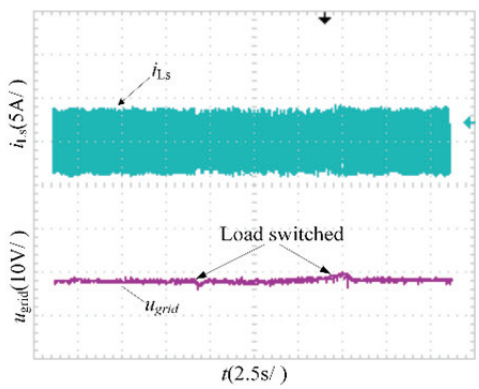

Fig. 14. Waveforms when the load is switched.

secondary control programs are working, the load resistor is switched, and the system can keep the output voltage and primary current stable. This shows that the control strategy in this paper works well. Thus, the output power is 672.4 W, and this experiment is done when the coils are without misalignment. Misalignment tolerance will be the key point of future research.

The load resistor R_L and the input DC voltage source E_{DC} are exchanged to explore the working condition of V2G. The DC voltage source imitates the vehicle, and R_L imitates the load of the power grid. Due to the independent constant current characteristics of the LCL resonant network [22], the source does not need control measures. In addition, the grid side can control bi-directional DC/DC according to the requirement.

Inverter waveforms of the voltage and current are shown in Fig. 13.

As can be seen in Fig. 13, the methods proposed in this paper can make the system works in the semi-soft switching state when power is transferring from vehicles to the grid. This figure also demonstrates the frequency stability of the proposed compensation network.

As can be seen in Fig. 14, the current i_{Ls} is kept constant, and the voltage of the grid can also be kept constant when the load is switched.

From the above experimental results, it can be seen that the proposed bi-directional WPT system is feasible, and that the control method is effective.

VI. Conclusions

In this paper, existing bi-directional WPT systems are analyzed. In an effort to solve the problems of existing systems, a current sourced bi-directional WPT system is proposed. According to the AC impedance, the working principle of the system is analyzed. The parameters configuration method with frequency stability are also given. To control the output voltage, a bi-directional DC/DC circuit is adopted on the grid side and independent boost of controllable rectifier bridge is used on the vehicles side. A control strategy based on "constant primary current, constant secondary voltage" is given, which is simple and easy to achieve. Finally, a small-scale experimental setup has been built to verify the effectiveness and feasibility of the proposed system.

Acknowledgment

This work was supported by the National High-technology R&D Program of China #2015AA016201.

References

[1] J. C. Mukherjee and A. Gupta, "A review of charge scheduling of electric vehicles in smart grid," *IEEE Syst. J.*, Vol. 9, No. 4, pp. 1541-1553, Dec. 2015.

[2] B.-J. Che, F.-Y. Meng, Y.-L. Lyu, W.-L. Zhu, K. Zhang, G.-H. Yang, J.-H. Fu, and L. Zhu, "Omnidirectional wireless power transfer system supporting mobile devices," *Applied Physics A: Materials Science & Processing*, Vol. 122, No. 2, pp. 54, Feb. 2016.

[3] O. Ellabban, J. V. Mierlo, and F. Lataire, "Control of a bidirectional Z-source inverter for electric vehicle applications in different operation modes," *J. Power Electron.*, Vol. 11, No. 2, pp. 120-130, Mar. 2011.

[4] F. Mwasilu, J. J. Justo, E.-K. Kim, T. D. Do, and J.-W. Jung, "Electric vehicles and smart grid interaction: A review on vehicle to grid and renewable energy sources

integration," *Renewable and Sustainable Energy Reviews*, Vol. 34, No. 2, pp. 501-516, Jun. 2014.
[5] H. Yoichi, "Novel EV society based on motor/ capacitor/ wireless - Application of electric motor, supercapacitors, and wireless power transfer to enhance operation of future vehicles," in *Proceeding of IMWS-IWPT*, pp. 3-8, 2012.
[6] K. Hartani, A. Merah, and A. Draou, "Stability enhancement of four-in-wheel motor-driven electric vehicles using an electric differential system," *J. Power Electron.*, Vol. 15, No. 5, pp. 1244-1255, Sep. 2015.
[7] A. Erdem, C. Kerim, C. Dariusz, and T. Bunyamin, "Efficiency analysis of a bi-directional DC/DC converter for wireless energy transfer applications," in *Proceeding of ECCE*, pp. 594-598, 2015.
[8] X. Dai, Y. Sun, Y.-G. Su, C.-S. Tang, and Z.-H. Wang, "Study on contactless power bi-directional push mode," *Proceedings of the CSEE*, Vol. 30, No. 18, pp. 55-61, Jun. 2010.
[9] U. K. Madawala and D. J. Thrimawithana, "A bidirectional inductive power interface for electric vehicles in V2G systems," *IEEE Trans. Ind. Electron.*, Vol. 58, No. 10, pp. 4789-4796, Oct. 2011.
[10] U. K. Madawala, and D. J. Thrimawithana, "Current sourced bi-directional inductive power transfer system," *IET Power Electron.*, Vol. 4, No. 4, pp. 471-480, Apr. 2011.
[11] X. Dai. H. Shi, and Y. Sun, "Study on LCL type composite resonant bi-directional power transfer mode," *J. Southwest Jiaotong Univ.*, Vol. 48, No. 3, pp. 487-493, May. 2013.
[12] J. Hua, H.-Z. Wang, Y. Zhao, and A.-L. Zhou, "LCL resonant compensation of movable ICPT systems with a multi-load," *J. Power Electron.*, Vol. 15, No. 6, pp. 1654-1663, Nov. 2015.
[13] F.-X. Yang, Y. Sun, and X. Dai, "Simulation of multi-load inductive coupled power bi-directional transfer mode," *Journal of Central South University (Science and Technology)*, Vol. 43, No. 10, pp. 3865-3871, Oct. 2012.
[14] P.-N. Pablo, R.-E. Agustin, and F. Silveira, "Bidirectional analysis and design of RFID using an additional resonant coil to enhance read range," *IEEE Trans. Microw. Theory Techn.*, Vol. 64, No. 7, pp. 2357-2367, Jul. 2016.
[15] Y. Zeng, H.-B. Chen, and R. Zhang, "Bidirectional wireless information and power transfer with a helping relay," *IEEE Commun. Lett.*, Vol. 20, No. 5, pp. 862-865, May. 2013.
[16] L. K. Gao, K. Zhou, W. J. Zhu, Z. D. Wu, Z. H. Wang, and X. Dai, "Design of energy feedback mode wireless charging system for electric vehicles," in *Proceeding of ICIEA*, pp. 1827-1831, 2013.
[17] M. D. Prete, A. Gostanzo, A. Georgiadis, A. Collado, D. Madotti, and Z. Popovic, "Energy-autonomous Bi-directional Wireless Power Transmission (WPT) and energy harvesting circuit," in *Proceeding of IMS*, pp. 1-4, 2015.
[18] U. Lee, K. D. Song, Y. Park, V. K. Varadan, and S. H. Choi, "Perspective in nanoneural electronic implants with wireless power-feed and sensory control," *J. Nanotechnol. Eng. Med.*, Vol. 1, pp. 021007, May 2015.
[19] A. J. Moradewicz and R. F. Miskiewicz, "Bidirectional inductive contactless energy transfer system topology for Electric Vehicles," in *Proceeding of IEVC*, pp. 1-7, 2014.
[20] J. Tritschler, B. Goeldi, S. Reichert, and G. Griepentrog, "Comparison of different control strategies for series-series compensated inductive power transmission systems," in *Proceeding of ECCE*, pp. 1-8, Oct. 2015.
[21] W. X. Zhong and S. Y. R. Hui, "Maximum energy efficiency tracking for wireless power transfer systems," *IEEE Trans. Power Electron.*, Vol. 30, No. 7, pp. 4025-4034, Jul. 2015.
[22] H. Hao, G. A. Covic, and J. T. Boys, "A parallel topology for inductive power transfer power supplies," *IEEE Trans. Power Electron.*, Vol. 29, No. 3, pp. 1140-1151, Mar. 2014.
[23] A. P. Hu, "Selected Resonant Converters for IPT Power Supplies," phD. Thesis, New Zealand, 2001.
[24] W. Zhang and C. C. Mi, "Compensation topologies of high-power wireless power transfer systems," *IEEE Trans. Veh. Technol.,* Vol. 65, No. 6, pp. 4768-4778, Jun. 2016.
[25] S. Li, W. Li, and J. Deng, "A double-sided LCC compensation network and its tuning method for wireless power transfer," *IEEE Trans. Veh. Technol.*, Vol. 64, No. 6, pp. 2261-2273, Jun. 2015.

Yue Sun received his B.E. degree in Electrical Engineering, his M.E. degree in Industry Automation and his Ph.D. degree in Mechanical Electrical Integrated Manufacturing from Chongqing University, Chongqing, China, in 1982, 1988 and 1995, respectively. In 1997, he was a Senior Visiting Scholar in France. He is presently working as a Professor in the State Key Laboratory of Power Transmission Equipment & System Security and New Technology, and in the College of Automation, Chongqing University. His current research interests include automatic control, wireless power transfer and power electronic applications.

Cheng Jiang received his B.E degree from the College of Automation, Chongqing University, Chongqing, China, in 2013, where he is presently working towards his Ph.D. degree in Control Theory and Control Engineering. His current research interests include wireless power transfer and power electronics.

Zhihui Wang received his B.E. and M.E. degrees from the College of Automation, and his Ph.D. degree in Control Theory and Control Engineering from the College of Automation, Chongqing University, Chongqing, China, in 2003, 2006 and 2009, respectively. He is presently working as an Associate Professor in the College of Automation, Chongqing University. His current research interests include both fundamental investigations and practical engineering applications in efficient high-power converters and wireless power supplies.

Lijuan Xiang received her B.E. degree in Automation from the College of Automation, Chongqing University, Chongqing, China, in 2012. From 2016 to 2017, she was a joint Ph.D. student in the College of Engineering, Pennsylvania State University, University Park, PA, USA. She is presently working towards her Ph.D. degree in Control Theory and Control Engineering from the College of Automation, Chongqing University. Her current research interests include wireless power transfer, the dynamic wireless charging of electric vehicles, power electronics and optimization algorithms.

Huan Zhang received his B.E. degree from the College of Automation, Southeast University, Nanjing, China, in 2013. He is presently working towards his M.E. degree in Control Theory and Control Engineering from the College of Automation, Chongqing University, Chongqing, China. His current research interests include wireless power transfer technology and power electronics.